Toward A Comprehensive Theory for the Sweeping of Trapped Radiation by Inert Orbiting Matter

Walker Fillius

Center for Astrophysics and Space Science

University of California, San Diego

Abstract

There is a need to calculate loss rates when trapped Van Allen radiation encounters inert orbiting material such as planetary rings and satellites. An analytic expression for the probability of a hit in a bounce encounter is available for all cases where the absorber is spherical and the particles are gyrotropically distributed on a cylindrical flux tube. The hit probability is a function of the particle's pitch angle, the size of the absorber, and the distance between flux tube and absorber, when distances are scaled to the gyroradius of a particle moving perpendicular to the magnetic field. Using this expression, we have computed hit probabilities in drift encounters for all regimes of particle energies and absorber sizes. This technique generalizes our approach to sweeping lifetimes, and is particularly suitable for attacking the inverse problem, where one is given a sweeping signature and wants to deduce the properties of the absorber(s).

1. INTRODUCTION

Planetary rings and satellites that are immersed in trapped radiation belts leave signatures in the surrounding radiation by decelerating and absorbing the energetic particles that strike their surfaces. *Alfven* [1942] realized long ago that this process would take place, and he gave it great importance in his theory of cosmogeny; but it was not until the space age, with *in situ* measurements at the outer planets, that these sweeping signatures drew widespread attention and became exploited as diagnostic tools for both the trapped radiation and orbiting material. Although some applications have depended only on the existence of sweeping signatures (e.g.: discovering new orbiting bodies [*Acuna and Ness,* 1976; *Fillius,* 1976; *Van Allen,* 1982; *Cheng et al.,* 1983] and inferring the symmetry properties of the Uranian magnetic field [*Stone et al.,* 1986]), others require quantitative computations of sweeping rates. These include quantifying the amount of orbiting material present in a ring [*Van Allen* 1987], and calculating trapped particle diffusion rates [*Hood,* 1983; *Thomsen et al.,* 1977; *Paonessa and Cheng,* 1986].

Simple considerations are sometimes adequate, but the quantitative computation of sweeping rates can be tricky, because the the geometry is complex and includes such complications as "leapfrogging" and "corkscrewing." Also, in general, one may have to range over orbiting material from submicron dust to nearly planet-sized masses, and thus consider intermediates and extremes of the relevant parameters. Previous papers have dealt with individual cases and used approximations applicable to restricted situations. Some of their results have been laborious and/or inaccurate. This paper is an attempt to fill the need for a method readily applicable to all cases.

Paonessa and Cheng [1985] make an excellent statement of the problem, and present many of the elements of a general theory. Our point of departure from their approach is that we have an analytic expression for the probability of absorption in a bounce encounter (See Section 3). This renders orbit tracing unnecessary, saving computation time, and identifies the parameter space in which we can carry out a general computation for the probability of absorption in a drift encounter (See Section 4). This general result

is highly suitable to use as a tool when dealing with the inverse problem; i.e.: given an absorption signature, deduce the properties of the unknown absorber. Also, we are now able to carry out the numerical computations to a higher degree of accuracy without being limited by the fineness of the grid and thus the computation time required. Before we present these results, Section 2 looks at several cases that can be worked out simply. This allows us to introduce the problem, and provides reference points to which we can compare the results to follow.

2. Straightforward Cases of Trapped Radiation Absorption

We assume that the orbiting material is electrically neutral, nonmagnetic, and too nonconductive to interact with the planetary magnetic field. Thus our problem is strictly geometric, with ample complexity contributed by the charged particle motion and the range of target sizes to be encompassed. There is usually enough randomness to justify a probabilistic approach, in which the loss rate, $\frac{-d\Phi}{dt}$, is proportional to the trapped particle density Φ divided by some lifetime τ:

$$\frac{d\Phi}{dt} = -\frac{\Phi}{\tau}. \tag{2.1}$$

There are straightforward arguments to obtain τ in several cases.

A Sparse Ring of Small Objects

Picture an annulus of width ΔR_p and circumference $2\pi R_p$ containing a collection of small objects of radius R much smaller than the particle gyroradius R_g. Let the sum of the objects' cross-sectional areas be A. If the objects are sparse, they do not overlap, and the opacity measured perpendicular to the ring plane is given simply by $\eta = \frac{A}{2\pi R_p \Delta R_p}$, with $\eta << 1$. Every time a trapped particle passes through the annulus, its chance of hitting one of the objects is $\frac{A}{2\pi R_p \Delta R_p cos\alpha}$, where α is the angle between the particle's trajectory and a normal to the ring plane.

When viewed in a magnetic coordinate system, the ring annulus might not be circular or centered on the planet, and the magnetic equator might not coincide with the ring plane. Consequently the distribution of ring material, dA/dL, may be unevenly spread over a range W of the magnetic coordinate L. Particles that are within W may or may not be within ΔR_p, depending upon their longitudes, as illustrated in Figure 2 of the paper by *Mogro-Campero and Fillius* [1976]. Rather than model the uneven distribution of dA/dL, we will use the average value, A/W. Additionally, we must consider that at some longitudes some particles will mirror at a lower magnetic latitude than the ring plane. Those particles that do not cross the ring plane in their bounce motion obviously escape absorption, at least for that fraction of their longitudinal motion. These approximations are best if the magnetic field is centered and aligned with the planetary spin axis, as at Saturn, and they are reasonable for small tilt and offset, as at Jupiter. Uranus will require special consideration, [*Paonessa and Cheng,* 1987].

We will let the particle lifetime be a longitudinal average, because for a sparse ring the trapped particles execute many longitudinal drift cycles during their residence time in W. With these simplifications the average time for a trapped particle to hit an absorber is

$$\tau_2 = \frac{T_b}{2\alpha_L} \frac{2\pi R_p W cos\alpha}{A}. \tag{2.2}$$

where T_b is the particle's bounce period, α_L is the fraction of bounces that cross the ring plane, as used by *Thomsen et al* [1977], and the reason for our choice of subscript on τ_2 will become apparent later. The lifetime for eliminating the particle from the sampled population is

$$\tau_3 = \nu\tau_2. \tag{2.3}$$

where ν is the average number of hits required. If a single hit is sufficient to annihilate the particle, then $\nu = 1$.

Fine Dust

Trapped particles in the energy ranges detected by the Pioneer and Voyager experiments will survive many hits on submicron-sized dust. To estimate ν when it is greater than one, consider a particle of given initial energy E. The critical number of hits ν(E) is

$$\nu(E) = \frac{R_{th}(E)}{n\bar{d}}. \tag{2.4}$$

where $\bar{d}$ is the average thickness of ring material traversed per hit, n is the density of the ring material in $gm\,cm^{-3}$, and R_{th}(E) is the particle's range above threshold in units of $gm\,cm^{-2}$. That is, R_{th}(E) is the amount of material the particle can traverse before its energy is reduced below the detector threshold, E_{th}:

$$R_{th}(E) = \int_E^{E_{th}} (-\frac{dE}{ndx})^{-1} dE. \tag{2.5}$$

where (-dE/ndx) is the energy loss rate of the particle in matter. For spherical objects of uniform radius R, $\pi R^2 \bar{d} = \frac{4}{3}\pi R^3$. Thus

$$\nu = \frac{R_{th}}{4/3nR}. \tag{2.6}$$

For a 1/2 MeV proton, R_{th} amounts to very little material, only about 10 microns of ice; for a 100 MeV proton, R_{th} is several centimeters; and for a 100 MeV electron, tens of centimeters.

A Large Object

For a sufficiently large satellite, absorption is inevitable whenever the drifting flux tube of the particle's gyromotion is intercepted by the satellite. This case is called "snowplow" absorption. The loss rate is still probabilistic, because the radial width, W, of the region where the particle might encounter the satellite is generally much greater than the effective diameter, d_{eff}, of the satellite, given by the satellite diameter plus two particle gyroradii, $d_{eff} = 2(R+R_g)$. If their relative drift motions bring particle and satellite to the same meridian with a relative period T_{rel}, then each time they pass

each other, the probability of absorption is given by $\alpha_L(d_{eff}/W)$, and so the absorption lifetime is

$$\tau_1 = \frac{T_{rel}}{\alpha_L} \frac{W}{d_{eff}}. \tag{2.7}$$

Comparison of Three Cases

As shown above, different absorber sizes lead to different formulas for the absorption lifetime. We collect the formulas here, to demonstrate their explicit dependence on R, α, and E.

$$\tau_1 = \frac{T_{rel}(\alpha, E)}{\alpha_L} \frac{W}{2(R + R_g(\alpha, E))}. \tag{2.8a}$$

$$\tau_2 = W R_p \frac{T_b(\alpha, E)}{\alpha_L} cos\alpha / R^2. \tag{2.8b}$$

$$\tau_3 = W R_p R_{th}(E) \frac{T_b(\alpha, E)}{\alpha_L)} cos\alpha / (4/3nR^3). \tag{2.8c}$$

The size of the absorber enters to the third power in equation (2.8c), the second power in (2.8b), and the first power in (2.8a). There is a ready physical explanation for this progression. An energetic particle passes right through fine dust, and the entire volume of the absorbing material acts to slow down the particle. If an object is bigger, a particle penetrates its skin only to a depth of R_{th}, being eliminated in a single hit, and it is the surface area that matters. Finally, if the object is yet bigger, its leading edge performs all the absorption, and it acts like a snowplow.

The transition from snowplow absorption described by equations (2.7) and (2.8a) to ring-like absorption described by equations (2.2) and (2.8b) takes place when the presence of the object in the particle's drift path is no longer sufficient to guarantee absorption. The particle might miss by one of two processes. In one process, often called "leapfrogging," the particle's drift velocity is high enough to carry it past the satellite during one half

of the bounce period. Similarly, in the other process the particle's bounce velocity is high enough to carry it past the satellite during a fraction of the gyrocircle that clears the satellite. This process is called "corkscrewing." The above treatment does not cover these possibilities, and in the past specialized numerical and Monte Carlo techniques have been used to deal with such complexities, [Bell and Armstrong, 1986; Paonessa and Cheng, 1985]. In section 3 we will present an analytic formula which covers corkscrewing, and in section 4 we will present a numerical calculation which covers leapfrogging and gives a result that can be applied to any case.

3. The Probability of a Hit in a Bounce Encounter

We need to distinguish between a bounce encounter and a drift encounter. This distinction is based on the usual decomposition of trapped particle motion into bounce and drift motion, and is valid because the drift period is much longer than the bounce period in all cases that concern us. One bounce encounter takes place as the charged particle moves from its last mirror point in one hemisphere, past the orbiting object, toward its next mirror point in the opposite hemisphere. Geometrically we represent the orbiting object as a sphere, and the particle's trajectory in the vicinity of the encounter as a spiral drawn on the surface of a cylindrical tube of magnetic flux. The bounce encounter produces a hit if the spiral intersects the sphere, and a miss if it doesn't. The problem is well-defined as soon as we specify the phase of the spiral and the distance between the cylinder and the sphere. However, we don't want to concern ourselves with any given phase; what we really want to know is what percentage of bounce encounters produce hits when the gyrophases are distributed uniformly. This is equivalent to assuming that the phase is random upon each bounce encounter and the particle motion is gyrotropic.

This geometry problem is solvable analytically as shown in Appendix A. We will use the letter p for the probability of a hit and q for the probability of a miss. The result is given below:

$$p = 1 - q = \phi_c/\pi \leq 1 \tag{3.1}$$

$$\phi_c = \phi_s + \frac{S}{R_g} tan^2\,\alpha\, sin\,\phi_s$$

$$cos\,\phi_s = -\frac{R_g}{S}\frac{1}{tan^2\alpha}\left\{1 - \sqrt{1 + tan^2\alpha\left[\left(\frac{S}{R_g}\right)^2 - \left(\frac{R}{R_g}\right)^2 + 1\right] + tan^4\alpha\left(\frac{S}{R_g}\right)^2}\right\}$$

where R is the radius of the sphere, S is the distance between the axis of the cylinder and the center of the sphere, R_g is the radius of the cylinder (i.e., the gyroradius), and α is the pitch angle, measured between the particle's velocity vector and a line parallel to the axis of the cylinder. Note that the distances R and S are scaled to the gyroradius, R_g. The condition, p$\leq$ 1, limits the probability to a maximum of 1, and merely reflects the fact that it is irrelevant if the spiral intersects the sphere more than once.

Equation (3.1) is easier to use if the distances are scaled to the gyroradius, a, that the same particle would have if its pitch angle were 90°. That is, $a = R_g/sin\alpha$. Then,

$$p = \phi_c/\pi \leq 1. \tag{3.2}$$

$$\phi_c = \phi_s + \sigma\frac{sin\alpha}{cos^2\alpha}\,sin\,\phi_s$$

$$cos\,\phi_s = -\frac{1}{\rho\, sin\alpha}\left\{cos^2\alpha - \sqrt{cos^2\alpha(1-\rho^2) + \sigma^2}\right\}$$

where σ = S/a, and ρ = R/a.

This function can be visualized by making contour plots of the hit probability in $\sigma - \rho$ space for a given value of α. Seven cases are shown in Figure 1(b-h). The cartoon in Figure 1(a) illustrates the relationship between object and flux tube in the four domains of $\sigma - \rho$ space. The divisions between domains occur, at the top, where $\sigma = \rho + \sin\alpha$;

at the lower left, where $\sigma = \sin\alpha - \rho$; and at the lower right, where $\sigma = \rho - \sin\alpha$. As depicted in the cartoon, at the upper left, the flux tube falls wide of the object, and the hit probability is zero. At the lower left, the flux tube circumscribes the object, and the hit probability is again zero. At the lower right, the flux tube is impaled in the object, and particles of all gyrophases hit the sphere. In the center, particles of some gyrophases hit the object and some don't, because of the corkscrew effect, and the phase-averaged hit probability is intermediate between zero and one. Equation 3.1 gives the same results as the numerically-computed Figure 2 of *Paonessa and Cheng* [1985]; however, we now have a more comprehensive view of the function.

4. The Probability of a Hit in a Drift Encounter

A drift encounter occurs once for every time the flux tube carrying the trapped particle passes the orbiting object in the direction of the orbital or drift motion. If the flux tube carrying the particle drifts around the planet with some period T_d, and the object has a Keplerian period T_k, then drift encounters occur with the period, T_{rel}, given by,

$$1/T_{rel} = 1/T_d - 1/T_k. \tag{4.1}$$

where negative periods correspond to retrograde motion. Three different drift encounters are depicted in Figures 2(a-c), using three representations for each case. In the first representation, at the left, the cross-sections of the absorber and of the flux tube carrying the particle are both drawn to scale. In the second representation, in the middle, the particle is represented only by the field line through its gyrocenter, and the absorber is drawn with an effective radius given by $R \pm R_g$. The third representation, at the right, shows what the encounter trajectory looks like in the $\sigma - \rho$ space of Figure 1. Here the position of the particle can be visualized as moving downward on the approach, until it reaches a minimum value of σ at the point of closest approach, and then returning upwards along the same path as it recedes. Although the flux tube carrying the particle

can be thought of as moving continuously past the object, bounce encounters occur only at discrete points along the path of the flux tube; for example: where dots are shown on the drift paths. Half a bounce period elapses between bounce encounters (half, because the bounce encounters alternate in direction). The half-bounce step size is obviously an important parameter, and we will call it H, or χ when normalized to the distance scale used above, so that χ = H/a. The three cases in Figure 2(a-c) span an order of magnitude in the relative dimensions of absorber and gyrocircle, and require different approximations from Section 2 above. Nevertheless, all bounce encounters can be calculated with equations (3.1) and (3.2), and the drift encounters are straightforward in $\sigma - \rho$ space.

No More Than One Bounce Per Drift Encounter

Note that when $H > 2(R + R_g)$, (or $\chi > 2(\rho + sin\alpha)$), the particle might pass the object without any bounce encounters at hazardous range ("leapfrogging"), and there can be at most one hazardous bounce during a drift encounter. In this case it is worthwhile to compute $\bar{p}$, the hit probability for bounce encounters averaged over the effective cross section of the object.

$$\bar{p} = \frac{\int_0^{\rho+sin\alpha} p(\sigma,\rho,\alpha)\, 2\pi\sigma\, d\sigma}{\pi(\rho + sin\alpha)^2}. \tag{4.3}$$

Figures 3(a and b) show $\bar{p}$, and $\bar{q}$ = 1 - $\bar{p}$, computed from (4.3) and (3.2), plotted as a function of ρ for a number of pitch angles, α.

If the drift encounters are suitably random, this is enough to arrive at the sweeping lifetime. We only need to count the number of hits per annihilation, and to remember that the probability given by equation (4.3) applies to bounce encounters that fall within the circle of radius ρ+sinα, whereas the sweeping lifetime applies to all particles within the annulus $2\pi R_p W$. Thus the hit probability is diluted by the ratio of these two areas:

$$\bar{\tau} = \nu \frac{T_b}{\bar{p}}\, R_p W/(a(\rho + sin\,\alpha))^2. \tag{4.4}$$

Equation (4.4) is valid for all corkscrew and leapfrog misses, but it does not allow for drift encounters with multiple bounces.

This result for $\bar{\tau}$ should agree with the results for ring absorption that we obtained in Section 2 under the additional approximations that we used then, namely when $R << R_g$ (or $\rho << sin\ \alpha$). Comparing Equation (4.4) with (2.2-3) and (2.8b-c), we find

$$\bar{p} = \frac{\rho^2}{sin^2\alpha\ cos\ \alpha},\ when\ \rho << sin\ \alpha. \tag{4.5}$$

This equation describes Figure 3 in the given limit.

More Than One Bounce Per Drift Encounter

When $H < 2(R + R_g)$ (or $\chi < 2(\rho + sin\ \alpha)$), there may be more than one bounce in the course of a drift encounter. With the assumption that the gyrophase is random upon each bounce encounter, the probability that a particle will survive one bounce is independent of all of the other bounces. Then the probability that a particle will survive the first i bounce encounters is given by the probability that it will survive up to the i^{th} bounce, multiplied by the probability that it will survive the i^{th} bounce encounter. By iteration, the probability, Q, that a particle survives the entire drift encounter is given by the product of the miss probabilities for all bounces in the drift encounter, and, since the probability, P, of a hit during the drift encounter is 1 - Q,

$$Q = \prod_i q_i \tag{4.6}$$

$$P = 1 - \prod_i (1 - p_i)$$

These products must be evaluated numerically. This computational task has been performed for individual cases by *Paonessa and Cheng,* [1985]. They marched each particle, bounce step by bounce step, past the absorbing object, evaluating p_i with each step, and accumulating the products as in equation (4.6). To get the average hit probability

for all drift encounters, they lined up N particles in a two-dimensional grid, of width $2(R+R_g)$ and depth H, marched them through, and averaged the drift probabilities,

$$\bar{Q} = \frac{1}{N}\sum_{j=1}^{N} Q_j \tag{4.7}$$

$$\bar{P} = \frac{1}{N}\sum_{j=1}^{N} P_j$$

Without an analytical method for evaluating p_i, however, this computational effort required tracing out a large number of spiral trajectories (e.g.: 360) on each bounce, and testing each for hits. Furthermore, it was necessary to do this separately for each named object and particle type. Equations (3.1) and (3.2) shorten this computational task and, best of all, make it possible to obtain a general result in terms of ρ, χ, and α. Let us show some partial results which illustrate the sweeping processes.

Absorption Profiles

Rairden [1980] calculated absorption profiles for the satellites of Saturn and a number of specific particle types. We are now in a position to generate a catalog of such profiles labeled in general coordinates. Figure 4 illustrates some of the range and variety that can occur. The 25 panels were calculated with five values for ρ (0.1, 0.316, 1.0, 3.16, and 10) and the same five values for χ, arranged so that rho increases from left to right, and χ increases from bottom to top. Each panel shows the probability of survival in a drift encounter for 10 values of pitch angle from 0 to 90° degrees. Although any profile has a width of $2(\rho + sin\ \alpha)$, we show only half because of symmetry.

To picture how these profiles were calculated, divide the distance from centerline to limb (0 to $\rho + sin\alpha$) into some number of intervals sufficient to resolve the level of detail, and envision this many columns of particles drifting toward the object. The columns must have a depth of H to cover the full range of bounce phases; but it helps to be clever in allocating the particles along this depth. We forecast which intervals from 0 to H have zero hit probability, and allocate the particles uniformly over the rest of the

interval, multiplying the average hit probability for these particles by the fraction of the full interval that they cover. This allocation is another geometry problem, and it is explained in Appendix B.

There are systematic differences in these profiles with χ, ρ, and α. At the right, where $R_g << R$, differences in pitch angle affect only the fringes of the profiles, and the reader will recognize this as the snowplow domain. By contrast, note the prominent differences in profile width where $R_g > R$ ($\rho < 1$), and recall that the width of each profile depends upon pitch angle through the gyroradius $R_g = a\ sin\ \alpha$. Leapfrogging is important where $\chi > \rho$, from the main diagonal to the upper left corner of the matrix, and is recognizable in the increased survivability as one scans from the bottom to the top of each column. A characteristic feature, when $\rho < 1$, is that absorption is higher near the edges of the profiles and lower near the center. The survival probability is improved near the center because the particles' gyromotion can carry them all the way around the absorber without hitting it, like a quoit around a peg. This effect was pointed out in our discussion of bounce encounters, in the lower left-hand corner of Figure 1. The reader will notice several profiles, for $\rho << 1$ and $\alpha = 90$, that have more than one minimum. These peculiar features arise from conjunctions of the half bounce step size, H, with the distance across the hazard. Appendix B demonstrates this phenomenon. It appears only for pitch angles near 90°, where the corkscrew effect is inoperative. At smaller pitch angles, corkscrew escapes smooth out the profiles and eliminate these complications. The strong pitch angle dependence for low values of rho is also a manifestation of the corkscrew effect.

Average Hit Probability

To obtain the average hit probability, $\bar{P}$, for all particles in the path of an absorber, it only remains to average over the width, $\rho + sin\alpha$, of the absorption profiles. The result is a function of χ, ρ and α, and may be exhibited as contour plots of $\bar{P}$ in $\chi - \rho$ space. We have computed $\bar{P}$, using the method explained above, for a number of pitch angles. Figure 5 illustrates some of the phenomenology this function exhibits in $\chi - \rho$ space. Figure

5(a) contrasts the two limits, $\alpha = 0°$ and 90°, and Figure 5(b) shows what happens for some intermediate values of the pitch angle. For $\rho >> 1$ the contours for different pitch angles are the same, as they should be, since here the gyroradius is negligible compared to the size of the absorber. The obvious difference in Figure 5(a) for $\rho < 1$ is caused by the difference in the radius of the flux tube covered by the particle's trajectory. For α of 0° and 90°, any object that touches the surface of the flux tube produces a hit, and the flux tube with the larger surface produces the larger hit probability. However, when the pitch angle deviates from the limit at 90°, corkscrew escapes become a possibility, and the hit probability falls off with decreasing pitch angle, as seen in Figure 5(b). The threshold for corkscrew escapes is roughly where the absorber fits inside the pitch of one spiral turn, [*Rairden,* 1980], or $R < \pi R_g cot\ \alpha$. In normalized coordinates, this criterion becomes $\rho < \pi cos\ \alpha$, which gives the positions where there are knees in the contours for intermediate pitch angles. At values of ρ to the left of these knees, the absorption probability falls off because of the corkscrew effect. The 25 dots in Figure 5(c) correspond to the 25 panels of Figure 4, and one can examine features in more depth by cross-comparing Figures 4 and 5.

5. The Average Absorption Lifetime

The absorption probability, $\bar{P}$, computed as in Section 4, and exhibited in Figure 5, pertains to each drift encounter. Then the average particle lifetime, $\bar{\tau}$, is,

$$\bar{\tau} = \frac{T_{rel}}{\bar{P}} \frac{W}{2\,a\,(\rho + sin\ \alpha)} \frac{\nu}{\alpha_L}. \tag{5.1}$$

using the terminology developed in Sections 2 and 3. This is a general equation which covers all cases, unlike equations 2.8(a- c).

To compare 5.1 to equations 2.8(a-c), note that 5.1 is a transparent extension of 2.8(a) for $\nu = 1$ and $\bar{P} = 1$. Equation 2.8(a) applies in the snowplow domain, which is the lower right hand sector of Figure 5. For ringlike sweeping described by equations 2.8(b) and (c),

recall that the application of these equations is restricted to $\rho << sin\,\alpha$, $\chi > 2(\rho + sin\,\alpha)$, and $\rho < \pi cos\,\alpha$. Then for 5.1 to be equivalent to 2.8(b) in this domain,

$$\bar{P} = \frac{\pi\rho^2}{2(\rho + sin\,\alpha)\chi\,cos\,\alpha}. \tag{5.2}$$

To get this result, we used the relationship $H/(2\pi R_p) = T_b/(2T_{rel})$. Equation 5.2 describes the upper left-hand section of Figure 5. This is easy to verify in the following limits,

$$\bar{P} = \frac{\pi\rho^2}{2\chi \sin\,\alpha\,cos\alpha},\ for\ \rho << sin\alpha. \tag{5.3a}$$

$$\bar{P} = \frac{\pi}{2}\frac{\rho}{\chi},\ for\ sin\alpha << \rho. \tag{5.3b}$$

The comparison with 2.8(b) applies also to 2.8(c), with the additional consideration that $\nu > 1$ for penetrable dust.

We see from the above that equation 5.1, using $\bar{P}$ calculated from equation 3.2 and the methods in Section 4, gives the same results as the straightforward cases presented in Section 2. However, we now have a solution for all of the non-straightforward cases, as well as a general formalism for understanding and interrelating the different regimes of particle sweeping from dust to planetoids.

6. DISCUSSION

Approximate Solutions

In Sections 2 and 4 we discussed approximations which are usable in certain cases. Having established χ, ρ, and α as the relevant parameters for determining sweeping probabilities, it is helpful to locate the domains of these approximations in $\chi - \rho$ space.

If there is no more than one bounce in a drift encounter, the average bounce probability, $\bar{p}$, suffices, where the relationship between $\bar{p}$ in equation (4.3) and $\bar{P}$ in (4.7) is the ratio of the areas over which bounce encounters have been averaged:

$$\frac{\bar{P}}{\bar{p}} = \frac{\pi(\rho + sin\,\alpha)}{2\chi}. \tag{6.1}$$

The criterion for this situation is $\chi > 2(\rho + sin\,\alpha)$, and is shown in Figure 5(c) for alpha = 0°, 30°, and 90°. Equations (4.3) and (4.4) are usable above this limit.

Snowplow absorption occurs when the absorber is much larger than either the gyroradius ($R >> R_g$) or the half-bounce step size ($R >> H$), and there are no corkscrew escapes ($R > \pi R_g\, cot\,\alpha$). These criteria are satisfied by the condition $\rho > \pi + 5\chi$, which is also drawn in Figure 5(c), cutting off the lower right-hand corner. Below this line, $\bar{P} \approx 1$, and as already noted in discussing Figure 4, this is the domain of snowplow absorption.

The straightforward case of ringlike absorption applies when $R_g >> R$, corkscrew escapes are possible ($R < \pi R_g\, cot\,\alpha$), and one can treat each bounce as independent statistically. This is approximately valid, for $\alpha = 30°$ and 90°, when $\rho < 0.1$ and $\rho < 0.2$, respectively, and the vertical lines define this domain on the left-hand edge of Figure 5(c).

Thus Figure 5(c) shows the ranges of the parameters χ , ρ, and, α where certain approximations simplify the task of calculating sweeping probabilities. The area of greatest difficulty is where the length scales are about equal; that is, near the diagonal where $\rho \approx \chi$, and also where ρ and $\chi \approx 1$. There are many cases for which simplification is not possible.

Applications

It is not our purpose in the present paper to investigate specific cases, as they are too extensive, differently motivated, and should be considered, each, individually. However, we want to demonstrate that our method is worthwhile, and provides a useful attack to sweeping computations. Therefore we will demonstrate how several cases studied in previous publications compare with our results. Figure 5(c) shows where Io (at Jupiter), and Dione and a putative shepherd for the G-ring (at Saturn) fall in $\chi - \rho$ space for protons and electrons of energies typically measured by spacecraft.

The positions on the two electron loci where χ approaches zero correspond to the well-

known resonance where the particles drift at the satellite's keppler velocity. Although $\bar{P}$ is unity for these cases, the absorption lifetime, $\bar{\tau}$, goes to infinity as expected because it is proportional to $T_{rel}/\bar{P}$ (equation 5.1).

Absorption of protons at Dione was examined intensively by *Paonessa and Cheng* [1985], computing everything numerically. These authors corrected the results of *Thomsen et al* [1977], and *Schardt and McDonald* [1983], who used approximations. Figure 5(c) confirms the need for numerical methods here.

Van Allen [1987] used an approximation to calculate absorption probabilities at the Saturnian G-ring, and concluded that the maximum possible radius for a single absorber at this position is 2.4 km. Such an object is shown, clearly in the ringlike approximation zone, in Figure 5(c). His approximation, equation (18) in his paper, is the same as our equation (2.2) if we use $2R_g$ for W, and $\alpha_L = 1$.

These values of χ and ρ were computed under the approximation that a particle's perpendicular gyroradius, a, has the same value everywhere on the absorber's orbital path. This approximation is excellent at Saturn, where the planetary magnetic field has near-perfect axial symmetry. At Jupiter, where the equivalent dipole has a small tilt and offset, it may vary by 15%, which would cause the loci in Figure 5(c) to be spread out slightly. However, at Uranus, the gyroradius may vary by a factor of two from one drift encounter to another, and a precise computation of the absorption lifetime will require further averaging to take this variation into account. Also, at Uranus, the half-bounce-step-size, H, will not be uniform for encounters at high magnetic latitude. For these reasons, Uranus requires a more complex computation for drift encounter absorption probabilities. However, the bounce encounter formulas given in this paper will shorten the process considerably.

Acknowledgement

This work was supported by NASA through grants NAS 2- 153, NGL 05-005-007, NAG W-336, and NAG W-652. I would like to thank Carl McIlwain for his encouragement during the preparation of this paper.

REFERENCES

Acuna, M.H., and N.F. Ness, "The Main Magnetic Field of Jupiter," *J. Geophys. Res., 81,* 2917-2922, June, 1976.

Alfven, H.,"On the Cosmology of the Solar System," *Stockholms Observatoriums Anneler, 14 (2),* 3-33, 1942.

Bell, E. V. II, and T. P. Armstrong, "Monte Carlo Simulation of Charged Particle Impact on the Satellites of Jupiter and Saturn," *J. Geophys. Res., 91* 1397-1403, Feb. 1, 1986.

Cheng, A.F., L.J. Lanzerotti, and C.G. MacLellan, "Does Saturn Have Rings Outside 10 Rs?" *Nature, 317,* 508-509, 10 October, 1985.

Fillius, W., "The Trapped Radiation Belts of Jupiter," in *Jupiter,* T. Gehrels, ed., Univ. Arizona Press, Tucson, 896-927, 1976.

Hood, L.L.,"Radial Diffusion in Saturn's Radiation Belts: A Modeling Analysis Assuming Satellite and Ring E Absorption," *J. Geophys. Res., 88,* 808-818, February 1, 1983.

Mauk, B.H., S.M. Krimigis, E.P. Keath, A.F. Cheng, T.P. Armstrong, L.J. Lanzerotti, G. Gloeckler, and D.C. Hamilton, "The Hot Plasma and Radiation Environment of the Uranian Magnetosphere," *J. Geophys. Res., 92,* 15,283-15,308, December 30, 1987.

Mogro-Campero, A., and W. Fillius,"The Absorption of Trapped Particles by the Inner Satellites of Jupiter and the Radial Diffusion Coefficient of Particle Transport," *J. Geophys. Res., 81,* March 1, 1976.

Paonessa, Mark and Andrew F. Cheng, "A Theory of Satellite Sweeping," *J. Geophys. Res. 90, A4,* 3428-3434, April 1, 1985.

Paonessa, M., and A.F. Cheng, "Limits on Ion Radial Diffusion Coefficients in Saturn's Inner Magnetosphere," *J. Geophys. Res., 91,* 1391-1396, February 1, 1986.

Paonessa, M., and A.F. Cheng, "Satellite Sweeping in Offset, Tilted Dipole Fields," *J. Geophys. Res., 92,* 1160-1166, Feb. 1, 1987.

Rairden, R., "Satellite Sweeping of Electrons and Protons in Saturn's Inner Magnetosphere," *University of Iowa Research Report 80-29,* 1980.

Schardt, A.W., and F.B. McDonald,"The Flux and Source of Energetic Protons in Saturn's Inner Magnetosphere," *J. Geophys. Res., 88,* 8923-8936, 1983.

Stone, E.C., J.F. Cooper, S.C. Cummings, F.B. McDonald, J.H. Trainor, N. Lal, R. McGuire, D.L. Chenette, "Energetic ChargedParticles in the Uranian Magnetosphere," *Science, 93-97, July 4, 1986.*

Thomsen, M.F., C.K. Goertz, and J.A. Van Allen, "On Determining Magnetospheric Diffusion Coefficients From the Observed Effects of Jupiter's Satellite Io," *J. Geophys. Res., 82,* 5541-5550, December 1, 1977.

Van Allen, J.A., "Findings on Rings and Inner Satellites of Saturn by Pioneer 11," *Icarus, 51,* 509-527, 1982.

Van Allen, J.A., "An Upper Limit on the Sizes of Shepherding Satellites at Saturn's Ring G," *J. Geophys. Res.,* 1153-1159, February 1, 1987.

FIGURE CAPTIONS

Fig. 1 The probability, p, of a hit in a bounce encounter, calculated from equation (3.2), for 7 values of the pitch angle, α. The contours correspond to values of p = 0.001, 0.1, 0.2, 0.3, 0.4, 0.5, 0.6, 0.7, 0.8, 0.9, and 0.999. See text, Section 3.

Fig. 2 Drift encounters (a-c) in three different representations (left to right).

Fig. 3 Bounce probabilities averaged over the effective disk of the absorber. These averages are useful if there can be no more than one bounce encounter in a drift encounter (i.e.: if H > $2(R+R_g)$). Fig 3(a): The probability of a hit in a bounce encounter, averaged over the effective disk of the absorber. Fig 3(b): The probability of a miss in a bounce encounter, averaged over the effective disk of the absorber.

Fig. 4 Twenty-five families of absorption profiles for as many locations in $\chi - \rho$ space. Each family includes profiles for 10 values of pitch angle from 0 through 90°. The ordinate in each panel is the probability of survival in a drift encounter (from 0 to 1), and the abscissa is the distance of the drift path from the center of the object (from 0 to $\rho + sin\,\alpha$).

Fig. 5(a) Contours of equal values for the average hit probability in a drift encounter, for two pitch angles, 0° and 90°.

Fig. 5(b) Contours of equal values for the average hit probability in a drift encounter, for four pitch angles, 30°, 60°, 75°, and 82.5°. The four pitch angles appear in the same order in each set.

Fig. 5(c) Loci in $\chi - \rho$ space for specific particles at the named absorbers: "A" represents protons at Dione; "B", protons at Io; "C", electrons at Dione; "D", electrons at Io; and, "E", protons at a putative 2.4 km radius satellite at the position of Saturn's G-ring. Particle energies are marked at 0.01, 0.1, 1.0, 10., 100., and 1000. MeV. Three pitch angles are shown. The 25 dots correspond to the positions in $\chi - \rho$ space of the 25 absorption profiles shown in Figure 4. The dashed and dotted lines delineate the portions of $\chi - \rho$ space where certain approximations are useful.

Fig. A1 Geometry of a bounce encounter.

Fig. A2 The surface of the flux tube that carries the spiraling particle. The phase is shown from 0 to 720° (two revolutions) in order to provide more continuity in the curves, and the z and $\rho - \phi$ directions are not to the same scale. The barberpole stripes describe the helical trajectories of particles, and the impact curve is the intersection of a spherical absorber with the flux tube.

Fig. B1 Representation of a drift encounter when $\rho = 0.1$ and $\chi = 1.0$.

APPENDIX A: DERIVATION OF THE PROBABILITY OF A HIT IN A BOUNCE ENCOUNTER

The absorbing object is a sphere of radius R, and the magnetic flux tube is a cylinder of radius R_g whose axis is a distance S from the center of the sphere (See Figure A1). The intersection of cylinder and sphere is easily solved. We will call it the impact curve since it is the locus where hits occur.

$$z^2 = R^2 - R_g^2 - S^2 + 2R_g S\, cos\phi. \qquad (A1)$$

Two cases are easily disposed of. No hits are possible unless $R_g - R < S < R_g + R$, which assures that the intersection exists. Also, if $0 < S < R - R_g$, the sphere engulfs the cylinder and all particles hit. Otherwise, we must describe the barberpole- stripe trajectory of a spiraling particle, which is,

$$z = \left(\frac{R_g}{tan\alpha}\right)(\phi - \phi_0). \qquad (A2)$$

Figure A2 shows what the surface of the cylinder looks like in two dimensions. Barberpole stripe a produces a hit; stripe c is a miss; and stripes b and d, which just osculate the impact curve, describe the boundaries between hits and misses. Our problem will be solved by a formula for these boundaries. Osculation occurs where the slope of the impact curve equals that of the barberpole stripe. Differentiating A1 and A2 and equating derivatives, the osculation locus is,

$$z = -S\, sin\phi tan\alpha. \qquad (A3)$$

The osculation points, (z_s, ϕ_s), occur at the intersections of the osculation locus with the impact curve, or the solution of A3 with A1.

$$cos\,\phi_s = -\frac{R_g}{S}\,\frac{1}{tan^2\alpha}\left\{1-\sqrt{1+tan^2\alpha\left[\left(\frac{S}{R_g}\right)^2-\left(\frac{R}{R_g}\right)^2+1\right]+tan^4\left(\frac{S}{R_g}\right)^2}\right\}$$

$$z_s = -S\,sin\phi_s tan\alpha. \qquad (A4)$$

We can then use A4 with A2 to solve for the phase limits for hits and misses.

$$\phi_c = \phi_s + \left(\frac{S}{R_g}\right) tan^2\alpha\, sin\phi_s. \qquad (A5)$$

APPENDIX B: GEOMETRICAL CONSIDERATIONS FOR THE ALLOCATION OF PARTICLES ALONG A DRIFT COLUMN

There are cases where the result would become grid limited if the particles were distributed uniformly from 0 to H. For instance, if $\chi >> \rho$, most of the candidate particles would leapfrog the object, missing altogether, and the hit probability would be based upon a reduced number of cases. Further, if $\rho << 1$, the absorber might even fall between consecutive grid points and be hit by none of the particles. In general, if the hit probability is 10^X, it will require at least 10^X grid points to evaluate it accurately. As our method is so general, it can encounter cases where these limitations apply. Although one can increase the number of grid points, brute force, it is more economical to forecast which intervals from 0 to H have zero hit probability, and allocate the candidate particles uniformly over the rest of the interval. One then calculates the average hit probability for these particles, and scales the result by the fraction of the full interval that they cover.

Figure A3 illustrates the geometry when $\rho = 0.1$ and $\chi = 0.316$. (The absorption profiles for this case are one of the families in Figure 4.) The drift encounter is drawn here as in the second representation of Figure 2; that is, the particle is represented by the field line through its gyrocenter, and the absorber, whose effective area is shaded by the diagonals that run from lower left to upper right, occupies an annulus with radii given by $R \pm R_g$. The particles to be followed through their drift encounters occupy the area of depth H and width $2(R_g + R)$ immediately above the annulus. The diagonal shading in this area that runs from upper left to lower right highlights the sections for which bounce hit probabilities must be computed. Particles in the unshaded areas have zero hit probabilities on all of the three bounces that it takes to drift past the absorber. The method of forecasting which particles are at risk is clear as soon as one realizes that, for any column at a given distance, b, from the centerline, there are no more than two intervals (inbound and outbound) where the drift path intersects the annulus. Each interval is projected, modulo H, from the annulus back to the initial column. The intervals can then be combined, if necessary, to eliminate overlap and accommodate contiguity.

It is interesting to note, in Figure A3, that the size of the risk interval has several

maxima and minima as a function of b; e.g.: there is a local maximum at b1, a local minimum at b2, another local maximum at b3, and a local minimum on the center line. These local extrema correspond to the peculiar variations in the 90° absorption profile from Figure 4, and now the reason for this effect is obvious. Since corkscrew misses are impossible for particles with a 90° pitch angle, any particle in the shaded area scores a hit; thus the hit probability is proportional to the shaded fraction of the drift column. This effect disappears after the pitch angle deviates far enough from 90° to allow the absorber to fit between consecutive arcs of the particle's spiral. Then the corkscrew effect diminishes the hit probability, and the peculiar shape of the profile is washed out.

ORIGINAL PAGE IS
OF POOR QUALITY

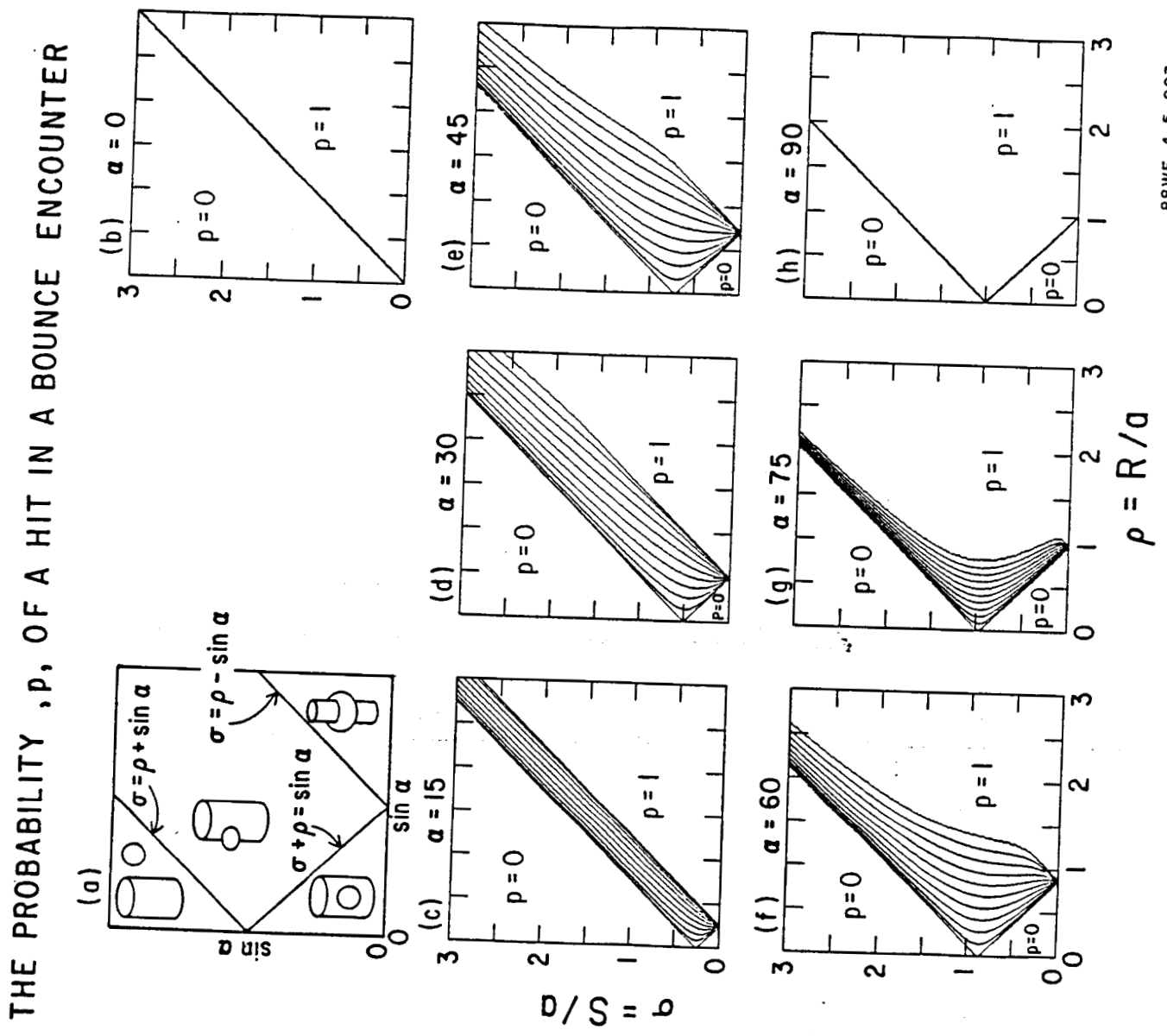

Fig.1

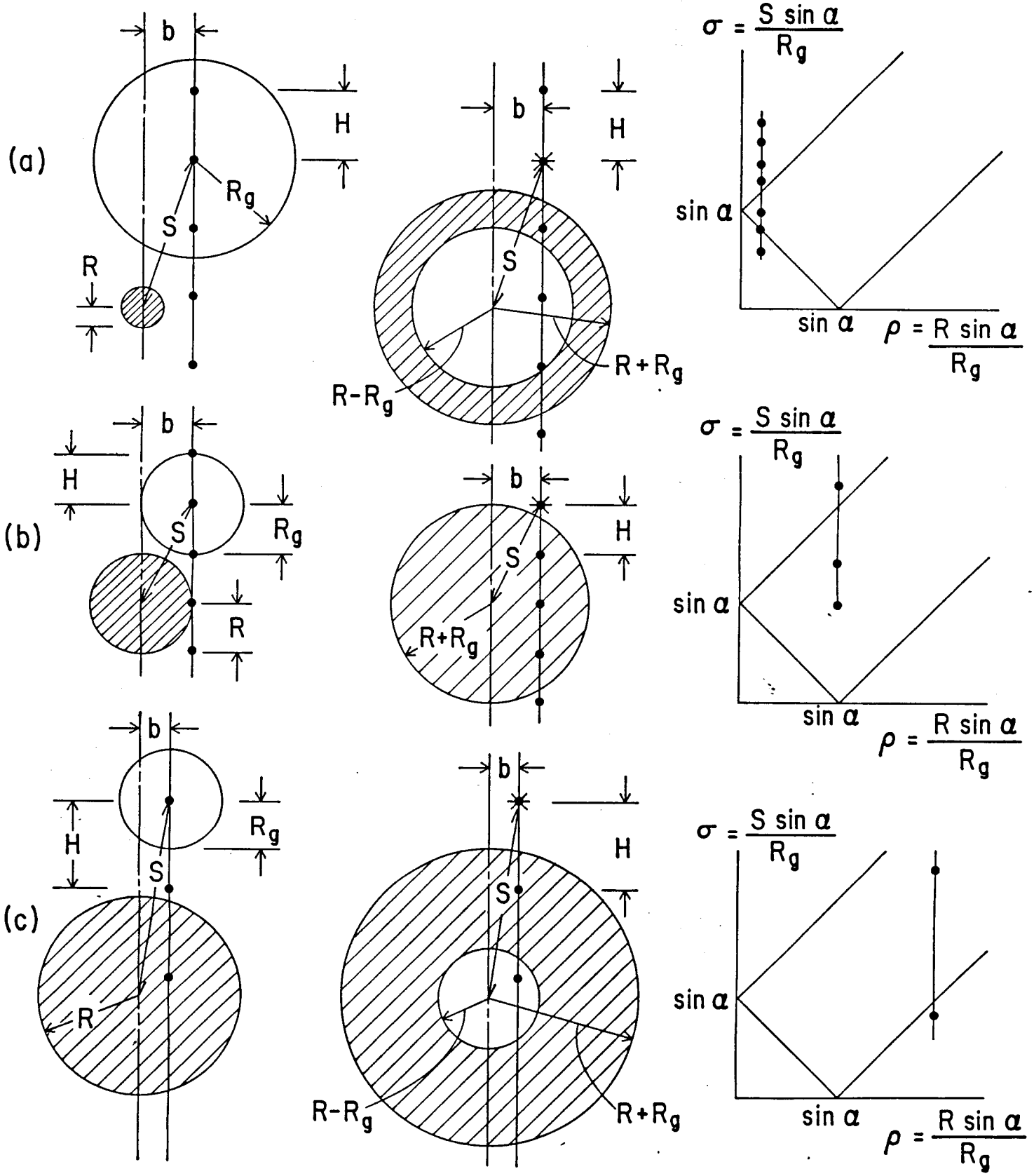

Fig.2

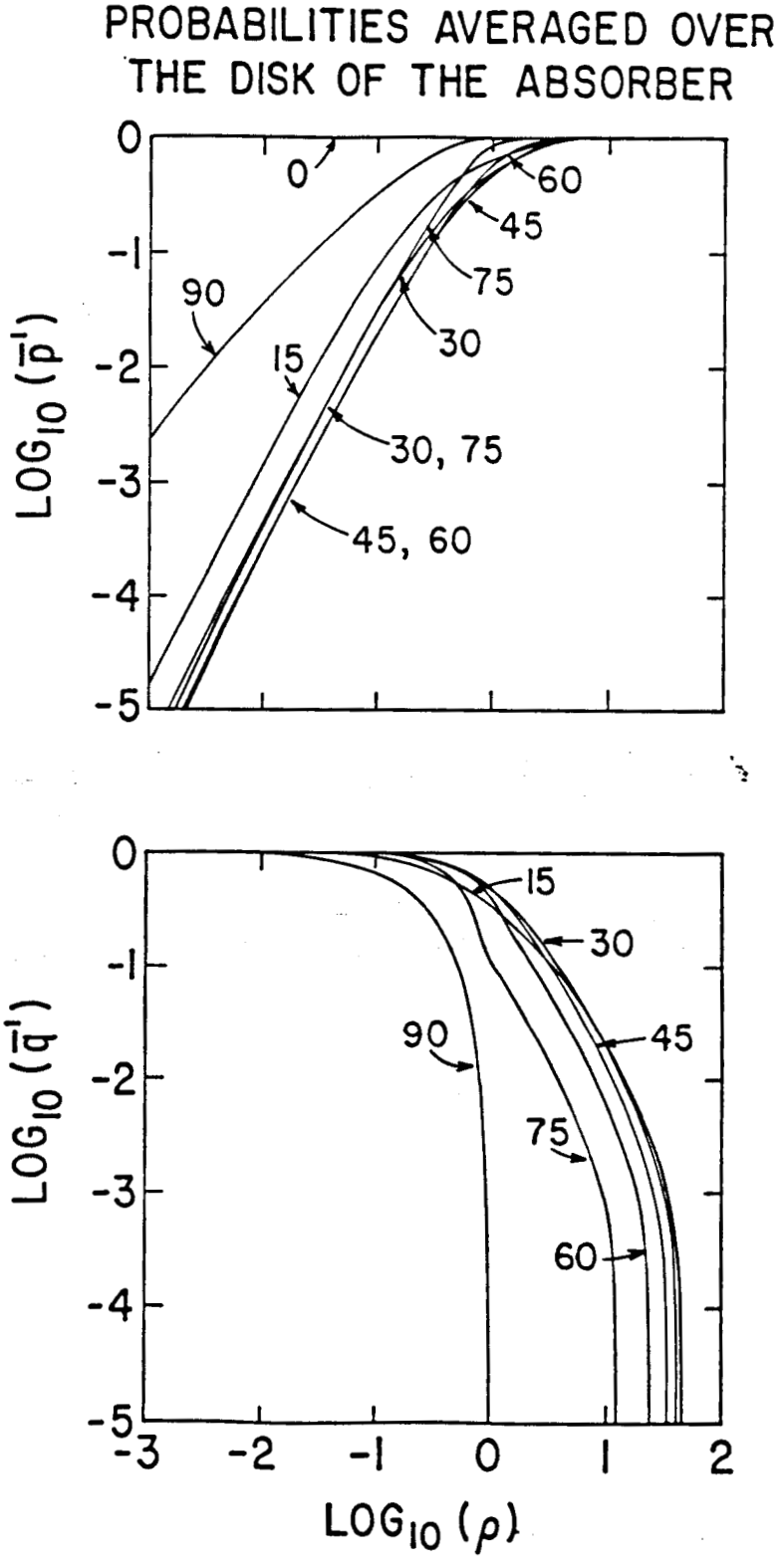
PROBABILITIES AVERAGED OVER
THE DISK OF THE ABSORBER
0
-1
-2
-3
-4
-5
LOG10 (p̄')
0
90
15
30, 75
45, 60
60
45
75
30
LOG10 (q̄')
15
30
45
90
75
60
-3
-2
-1
0
1
2
LOG10 (ρ)
88WF-4,5-010

Fig.3

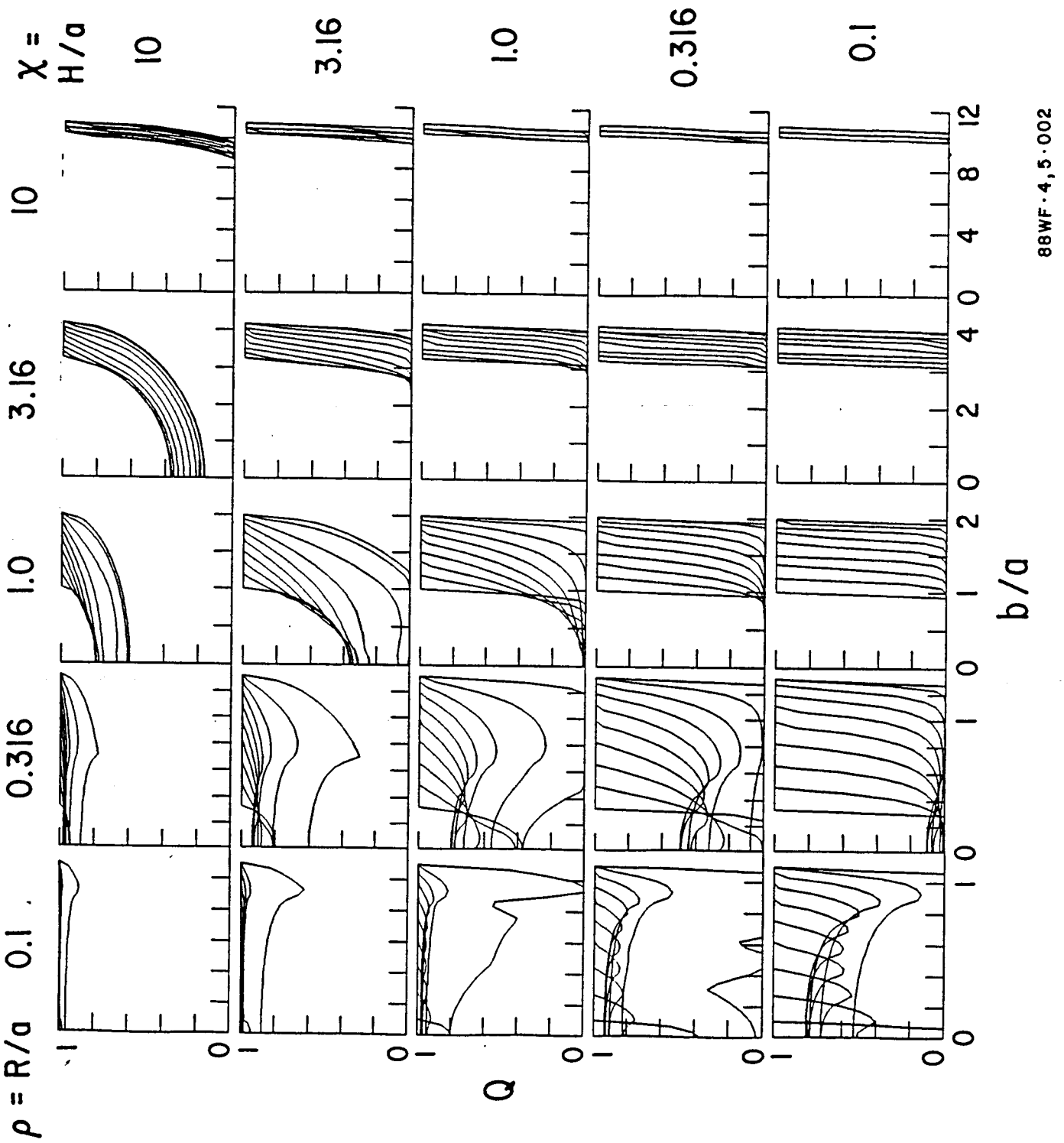

Fig.4

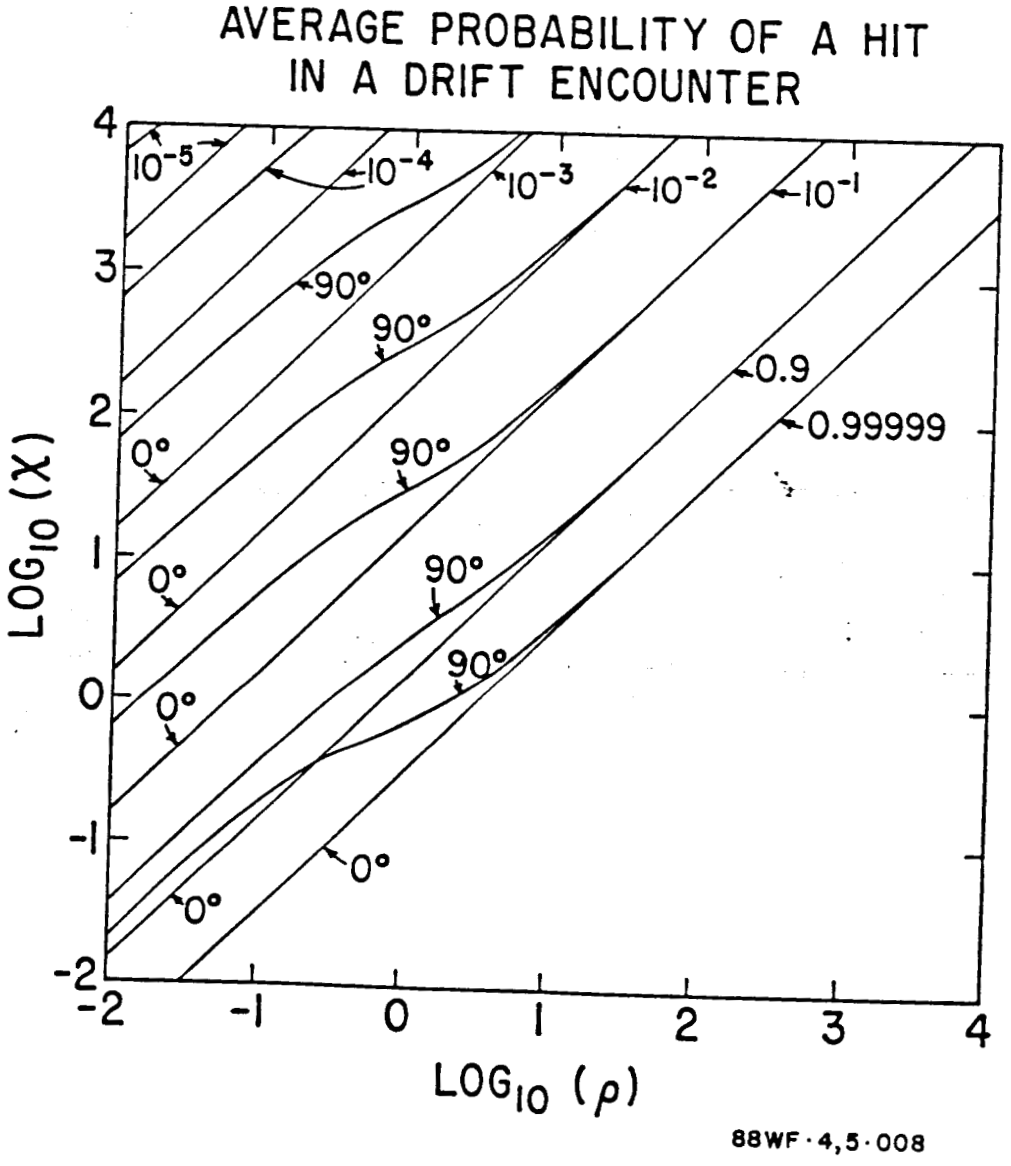
AVERAGE PROBABILITY OF A HIT
IN A DRIFT ENCOUNTER
10^{-5}
10^{-4}
10^{-3}
10^{-2}
10^{-1}
90°
90°
90°
90°
90°
0°
0°
0°
0°
0°
0.9
0.99999
$LOG_{10}(\chi)$
$LOG_{10}(\rho)$
88WF·4,5·008

Fig.5a

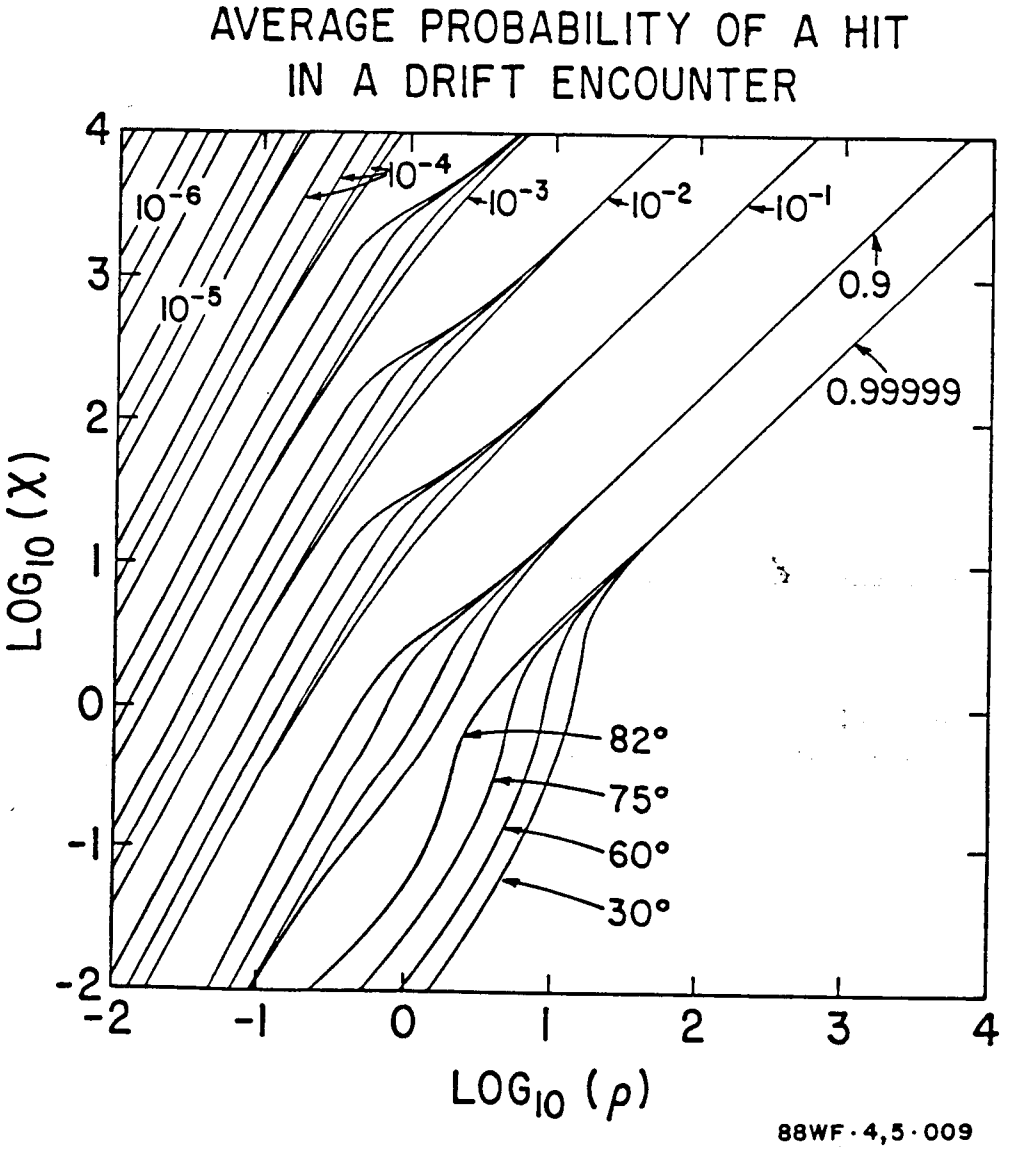
AVERAGE PROBABILITY OF A HIT
IN A DRIFT ENCOUNTER
10^{-6}
10^{-5}
10^{-4}
10^{-3}
10^{-2}
10^{-1}
0.9
0.99999
82°
75°
60°
30°
$LOG_{10}(X)$
$LOG_{10}(\rho)$
88WF·4,5·009

Fig.5b

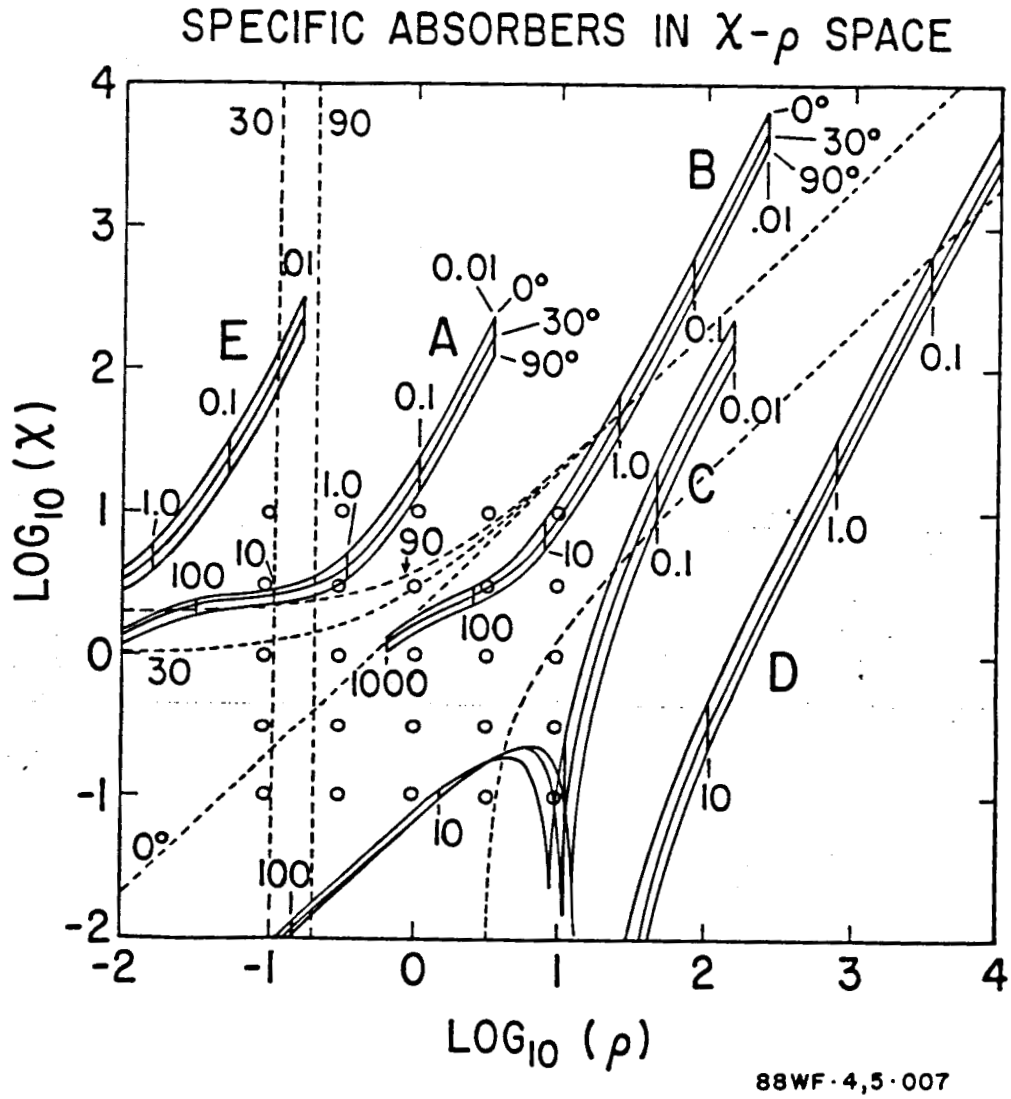
SPECIFIC ABSORBERS IN X-ρ SPACE
LOG10 (X)
LOG10 (ρ)
A
B
C
D
E
0°
30°
90°
88WF·4,5·007

Fig.5c

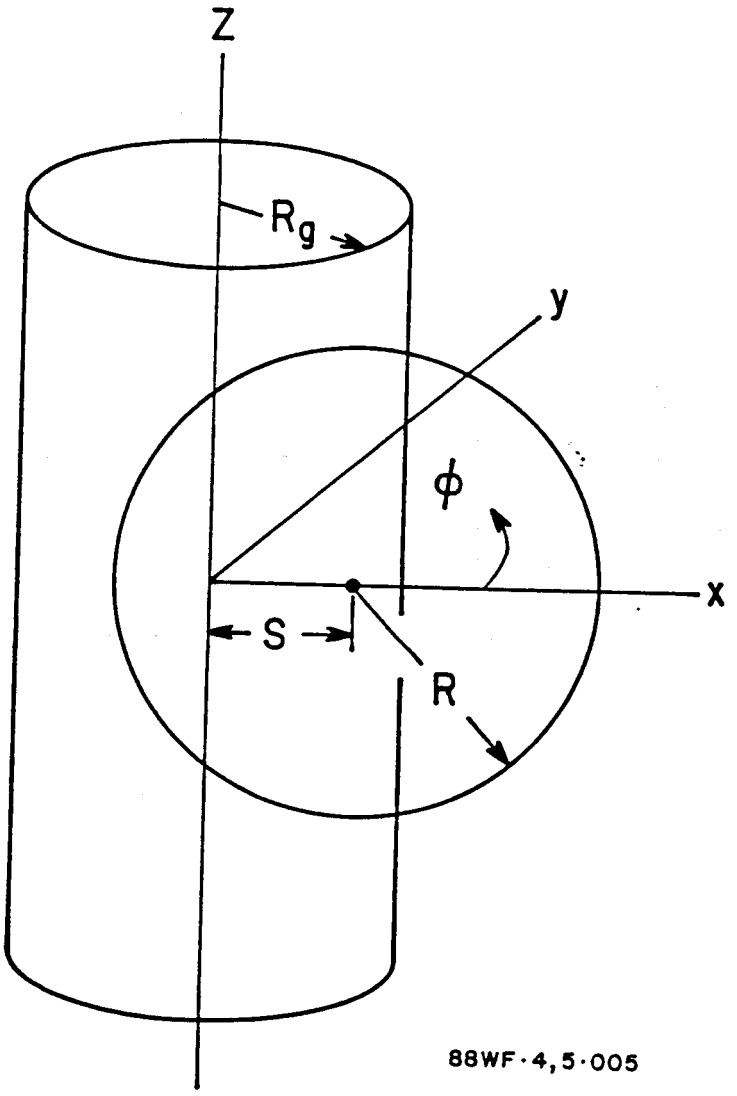

Fig.A1

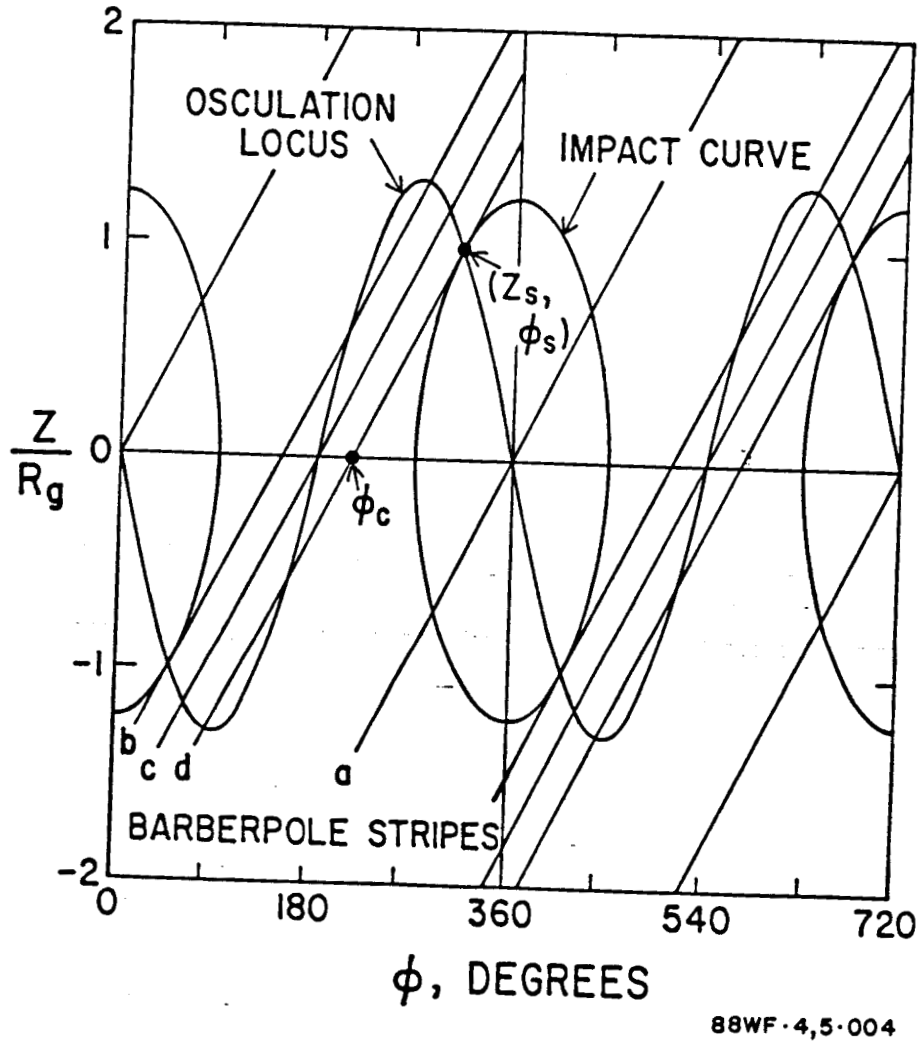
OSCULATION LOCUS
IMPACT CURVE
(Z_s, ϕ_s)
ϕ_c
$\frac{Z}{R_g}$
2
1
0
-1
-2
b
c
d
a
BARBERPOLE STRIPES
0
180
360
540
720
ϕ, DEGREES
88WF-4,5-004

Fig.A2

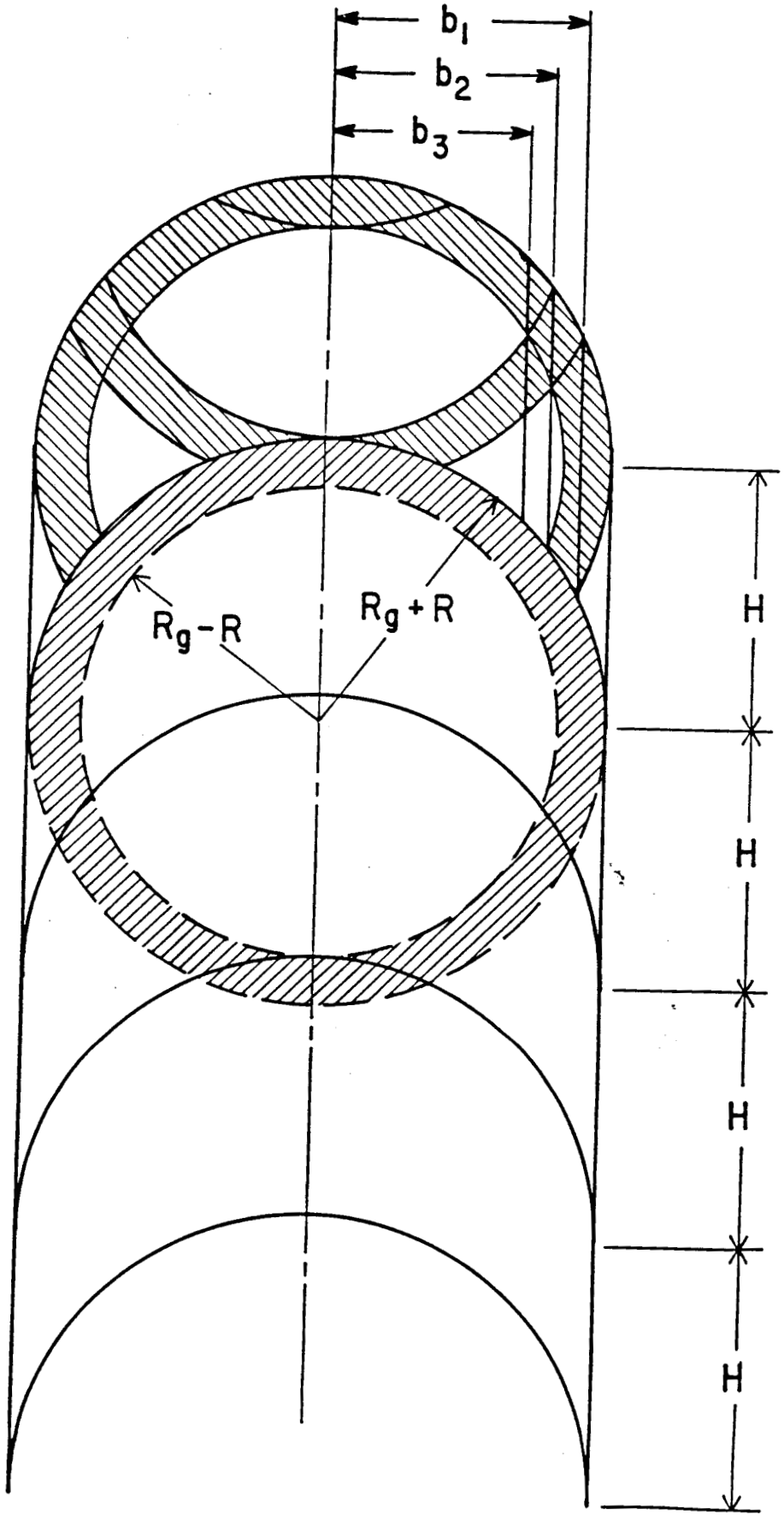

88WF·4,5·006

Fig.B1